

ADAPTIVE SHRINKAGE ESTIMATION FOR PERSONALIZED DEEP KERNEL REGRESSION IN MODELING BRAIN TRAJECTORIES

Vasiliki Tassopoulou^{1,2}, Haochang Shou^{1,3}, and Christos Davatzikos^{1,2}

¹Center for AI and Data Science for Integrated Diagnostics, University of Pennsylvania

²Department of Bioengineering, University of Pennsylvania

³Department of Biostatistics, Epidemiology and Informatics, University of Pennsylvania

{vasiliki.tassopoulou, hshou, christos.davatzikos}@pennmedicine.upenn.edu

ABSTRACT

Longitudinal biomedical studies monitor individuals over time to capture dynamics in brain development, disease progression, and treatment effects. However, estimating trajectories of brain biomarkers is challenging due to biological variability, inconsistencies in measurement protocols (e.g., differences in MRI scanners) as well as scarcity and irregularity in longitudinal measurements. Herein, we introduce a novel personalized deep kernel regression framework for forecasting brain biomarkers, with application to regional volumetric measurements. Our approach integrates two key components: a *population* model that captures brain trajectories from a large and diverse cohort, and a *subject-specific* model that captures individual trajectories. To optimally combine these, we propose *Adaptive Shrinkage Estimation*, which effectively balances population and subject-specific models. We assess our model’s performance through predictive accuracy metrics, uncertainty quantification, and validation against external clinical studies. Benchmarking against state-of-the-art statistical and machine learning models—including linear mixed effects models, generalized additive models, and deep learning methods—demonstrates the superior predictive performance of our approach. Additionally, we apply our method to predict trajectories of composite neuroimaging biomarkers, which highlights the versatility of our approach in modeling the progression of longitudinal neuroimaging biomarkers. Furthermore, validation on three external neuroimaging studies confirms the robustness of our method across different clinical contexts. We make the code available at <https://github.com/vatass/AdaptiveShrinkageDKGP>.

1 INTRODUCTION

Accurately predicting the temporal progression of brain biomarkers is essential for monitoring disease progression and determining optimal intervention points (Maheux et al., 2023). However, challenges such as biological variability among individuals, limited longitudinal data, and irregular observation intervals make model development particularly difficult. Since accurate and reliable predictions are imperative, models must dynamically adapt as new subject-specific data become available, ensuring personalized predictions.

Several predictive models have been proposed to model the progression of biomarkers in the field of neuroimaging (Marinescu et al., 2018). Traditional methods, such as linear mixed effects models (Lindstrom & Bates, 1988), often struggle to handle high-dimensional multivariate data effectively and are predominantly used for statistical inference (Bernal-Rusiel et al., 2013; Xie et al., 2023). Additionally, mixed-effect regression modeling is commonly employed to address longitudinal predictions by fitting biomarker progression to linear or sigmoidal curves (Sabuncu et al., 2014; Koval et al., 2021). However, this approach may be limited by its reliance on predefined trajectory shapes. More recently, Hong et al. (2019) and Gruffaz et al. (2021) explored manifold learning techniques to capture biomarker trajectories requiring subjects with at least two acquisitions for inference. Additionally, Lorenzi et al. (2019) introduced a Gaussian process-based disease progression model capable of predicting biomarkers like cognitive scores and volumetric measurements, but it relies

on specific design assumptions regarding the number of observations per subject and also uses low-dimensional input (i.e, five biomarkers). In the same spectrum, Koval et al. (2021) presented a Bayesian mixed effects model for estimating biomarker trajectories from low-dimensional inputs. Abi Nader et al. (2020) proposed a method for spatiotemporal progression of biomarkers without adapting to subject’s follow-up. Tassopoulou et al. (2022) proposed a deep kernel regression method to infer biomarker trajectories from high-dimensional multivariate imaging features, though it does not utilize individual subject trajectories to refine predictions. In a related direction, Rudovic et al. (2019) developed a meta-weighting scheme combining two personalized Gaussian process models to forecast ADAS-Cog13 (Mohs et al., 1997) scores up to two years ahead. Similarly, Chung et al. (2019) introduced a deep mixed effects framework for personalization in electronic health record time-series data, employing a long short-term memory network (Hochreiter & Schmidhuber, 1997) to model population trends while using a Gaussian process to capture subject-specific deviations.

In this paper, we address the above limitations by proposing *Deep Kernel Regression with Adaptive Shrinkage Estimation*, a composite framework for predicting longitudinal brain trajectories leveraging all the available observations of the test subject, either single acquisition or multiple randomly-timed acquisitions. Unlike previous approaches that predict biomarkers within predetermined time intervals (Rudovic et al., 2019), our method is designed to forecast over a practically unbounded future time horizon while simultaneously refining past observations by reducing noise in subject-specific observations. This dual capability enhances measurement reliability and preserves the global progression trend from the initial observation to any unseen future time point. Moreover, our framework naturally handles randomly-timed and temporally unaligned longitudinal observations without requiring imputation, thereby leveraging all available data. By extending the shrinkage estimator concept from Bayesian statistics and penalized inference (James & Stein, 1961; Shou et al., 2014), our method learns weights to combine population and subject-specific deep kernel model through an adaptive shrinkage estimator, while accounting for both observation time and predictive uncertainty.

Contributions. **1)** We propose a novel deep kernel regression framework for predicting biomarker trajectories from sparse longitudinal observations, that maps high-dimensional, imaging and clinical features into a lower-dimensional latent space predictive of biomarker progression. Our approach naturally accommodates randomly-timed and temporally unaligned observations without requiring imputation. **2)** We introduce Adaptive Shrinkage Estimation that fuses population and subject-specific model. This framework enables incremental updates to personalized predictions as new data arrive and it also refines historical observations to reduce noise while preserving the overall progression trend from the first observation to any future time. Importantly, the adaptive shrinkage estimator is interpretable, offering insights into the relative contributions of population and subject-specific model. **3)** We showcase the versatility of our method to be applied for the prediction of two additional composite neuroimaging biomarkers from high-dimensional multivariate imaging data and clinical covariates. **4)** We demonstrate the generalizability of our method in different clinical contexts, showing its ability to generalize in three external clinical studies.

2 METHOD

2.1 PROBLEM FORMULATION

We address the problem of predicting biomarker trajectories, modeled as a one-dimensional signal spanning multiple years. Formally, biomarker progression is described by the function $f : U \rightarrow Y$, where $U \in \mathbb{R}^K$ and $Y \in \mathbb{R}$. The input is represented as $\mathbf{U} = (X, M, T)$, where X denotes the imaging features, M denotes the clinical covariates at subject’s first visit, and T represents the temporal variable, indicating time in months from the first visit. The biomarker trajectory is denoted as $Y = (y_0, y_1, \dots, y_n)$, corresponding to the biomarker values at time points $T = (t_0, t_1, \dots, t_n)$. Our goal is to learn smooth functions biomarker progression using imaging and clinical data. To achieve this, we employ Deep Kernel Learning (DKL) (Wilson et al., 2015). The deep kernel integrates imaging and clinical covariates, learning a lower-dimensional representation informative for biomarker progression, while a Gaussian Process (GP) models the temporal dependencies. The backbone model, Deep Kernel Gaussian Process (DKGP), is defined as: $f(\mathbf{U}) \sim \mathcal{GP}(\mu, \mathbf{K}(\Phi(\mathbf{U}), \Phi(\mathbf{U})))$, where Φ is a transformation function.

2.2 POPULATION DEEP KERNEL MODEL (P-DKGP)

The population model leverages data from the population dataset $D_p = \{\mathbf{U}_p, \mathbf{Y}_p\}$, comprising subjects with longitudinal observations. It applies the transformation $\Phi(u; \mathbf{W}, \mathbf{b})$, a Multi-Layer

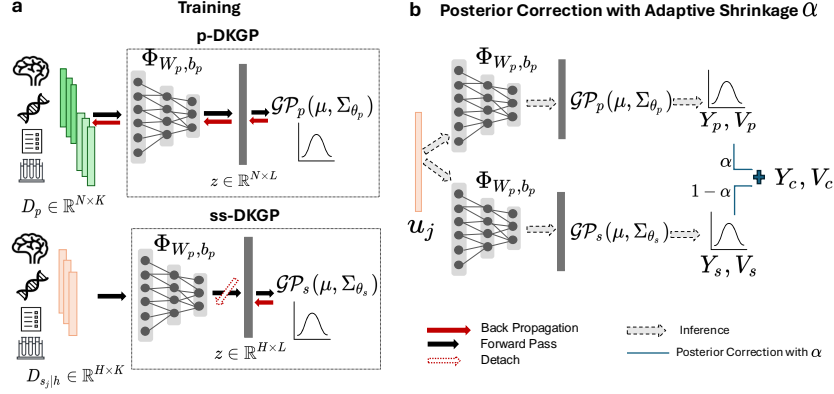


Figure 1: Overview of the proposed framework. In Figure 1a, we illustrate the training process of the two models, p-DKGP and ss-DKGP. The population dataset D_p contains multiple longitudinal acquisitions of subjects, where N is the total number of samples across all subjects, and L is the latent dimension obtained from transformation Φ . Different shades of green in the population dataset indicate different subjects in D_p . We denote the observed trajectory of subject j with h samples as $D_{s_j|h}$. These samples are utilized to train the ss-DKGP. During the training of the ss-DKGP, the transformation Φ is fixed, and only the subject-specific Gaussian process is optimized. In Figure 1b, we describe the personalization process through the shrinkage parameter α . For subject j , we extrapolate biomarker values over time using both the p-DKGP and ss-DKGP models. These extrapolated values are then used to infer the adaptive shrinkage α for posterior correction, yielding the personalized posterior predictive mean Y_c variance V_c of the subject’s trajectory.

Perceptron (MLP), that maps the input data $\mathbf{U}_p = (X, M, T)$ into a latent representation:

$$\mathbf{Z}_p = \Phi(\mathbf{U}_p; \mathbf{W}, \mathbf{b}). \quad (1)$$

A GP, subsequently, models the biomarker progression function f using a Radial Basis Function (RBF) kernel as the covariance function and a zero mean: $f(\mathbf{Z}_p) \sim \mathcal{GP}(0, K(\mathbf{Z}_p, \mathbf{Z}_p'))$.

The population parameters $\gamma_p = \{\mathbf{W}_p, \mathbf{b}_p, l_p, \sigma_p^2, \sigma_{n_p}^2\}$ include both the transformation parameters of Φ and the Gaussian Process (GP) hyperparameters: the lengthscale l_p , signal variance σ_p^2 , and noise variance $\sigma_{n_p}^2$. These parameters are jointly learned by maximizing the Marginal Log Likelihood (MLL) of the GP (Wilson et al., 2015; Rasmussen & Williams, 2006).

For a test subject j with input $u_j = (x_j, m_j, t)$, we denote the transformed input as $z_j = \Phi(u_j; \mathbf{W}_p, \mathbf{b}_p)$.

The posterior predictive distribution of the biomarker function at point $u_j = (x_j, m_j, t)$ is:

$$f_{p_j} | (\mathbf{Z}_p, \mathbf{Y}_p), z_j \sim \mathcal{N}(\bar{\mathbf{f}}_{p_j}, \text{cov}(\mathbf{f}_{p_j})). \quad (2)$$

The mean and variance of the predictive posterior distribution provide the predictions and their uncertainties, respectively, and are calculated as follows:

$$\bar{\mathbf{f}}_{p_j} = \mathbb{E}[\mathbf{f}_* | \mathbf{Z}_p, \mathbf{Y}_p, z_j] = K(z_j, \mathbf{Z}_p)[K(\mathbf{Z}_p, \mathbf{Z}_p) + \sigma_{n_p}^2 I]^{-1} \mathbf{Y}_p, \quad (3)$$

$$\text{Var}(\mathbf{f}_{p_j}) = K(z_j, z_j) - K(z_j, \mathbf{Z}_p)[K(\mathbf{Z}_p, \mathbf{Z}_p) + \sigma_{n_p}^2 I]^{-1} K(\mathbf{Z}_p, z_j), \quad (4)$$

where $\sigma_{n_p}^2$ is the additive independent identically distributed Gaussian noise ϵ .

For simplicity, the predictive mean and variance of a biomarker for test subject j from the p-DKGP are denoted as y_p and v_p , respectively. By prompting the p-DKGP model with different time intervals t , yields the predicted trajectory and predictive uncertainty across time, represented as $Y_p = (y_{p1}, y_{p2}, \dots, y_{pT})$ and $V_p = (v_{p1}, v_{p2}, \dots, v_{pT})$.

2.3 SUBJECT-SPECIFIC DEEP KERNEL MODEL (SS-DKGP)

For a new test subject, let h denote the number of observations and T_{obs} the time of observation from the initial acquisition. The observed data for the subject is represented as $D_s = \{(X_s, M_s, T_s), Y_s\}$. The ss-DKGP model is trained on D_s to capture the subject-specific trajectory. The transformation $\Phi(\cdot; \mathbf{W}_p, \mathbf{b}_p)$, learned via the p-DKGP, initializes the deep kernel of the subject-specific model.

We initialize a new GP with an RBF kernel and a zero mean. During the training of the ss-DKGP, only the observed trajectory of the subject is used. Specifically, we update the GP hyperparameters, which include the length-scale l_s and the signal variance σ_s , while keeping the weights of the function $\Phi(\cdot; \mathbf{W}_p, \mathbf{b}_p)$ frozen during backpropagation. The subject-specific GP hyperparameters $\gamma_s = \{l_s, \sigma_s^2, \sigma_{n_s}^2\}$ are jointly learned by maximizing the MLL of the GP.

For subject j with input $u_j = (x_j, m_j, t)$, we denote their transformation as $z_j = \Phi(u_j; \mathbf{W}_p, \mathbf{b}_p)$.

The posterior predictive distribution of the biomarker progression function at time point t is:

$$f_{s_j} | (\mathbf{Z}_s, \mathbf{Y}_s), z_j \sim \mathcal{N}(\bar{\mathbf{f}}_{s_j}, \text{cov}(\mathbf{f}_{s_j})), \quad (5)$$

where $z_j = \Phi(u_j; \mathbf{W}_p, \mathbf{b}_p)$

The predictive mean and variance, representing the predictions and their associated uncertainties respectively, are computed as follows:

$$\bar{\mathbf{f}}_{s_j} = \mathbb{E}[\mathbf{f}_{s_j} | \mathbf{Z}_s, \mathbf{Y}_s, z_j] = K(z_j, \mathbf{Z}_s)[K(\mathbf{Z}_s, \mathbf{Z}_s) + \sigma_{n_s}^2 I]^{-1} \mathbf{Y}_s, \quad (6)$$

$$\text{Var}(\mathbf{f}_{s_j}) = K(z_j, z_j) - K(z_j, \mathbf{Z}_s)[K(\mathbf{Z}_s, \mathbf{Z}_s) + \sigma_{n_s}^2 I]^{-1} K(\mathbf{Z}_s, z_j). \quad (7)$$

where $\sigma_{n_s}^2$ is the additive independent identically distributed Gaussian noise ϵ .

For simplicity, the predictive mean and predictive variance of the ss-DKGP are denoted as y_{s_j} and v_{s_j} , respectively. By querying the ss-DKGP model at different time intervals t we reconstruct the biomarker trajectory of subject j , yielding the predicted trajectory $Y_s = (y_{s_1}, y_{s_2}, \dots, y_{s_T})$ and predictive uncertainty $V_s = (v_{s_1}, v_{s_2}, \dots, v_{s_T})$.

2.4 PREDICTIVE POSTERIOR CORRECTION

Given predictions y_p and y_s from the p-DKGP and ss-DKGP models, the personalized prediction is expressed as a linear combination:

$$y_c = \alpha y_p + (1 - \alpha) y_s, \quad (8)$$

where, α is the shrinkage parameter reflecting the relative confidence in each model. Assuming independence between the models, the combined prediction y_c retains Gaussian properties, and its variance is given by:

$$v_c = \alpha^2 v_p + (1 - \alpha)^2 v_s. \quad (9)$$

In Supplementary Section 2.4 we address the independence assumption and its impact.

The weights α and $1 - \alpha$ quantify the credibility of each model, yielding a new posterior predictive mean Y_c and variance V_c . Values of α close to 1 indicate higher confidence in p-DKGP model, while values close to 0 reflect greater trust in ss-DKGP model. We refer to α as the shrinkage parameter.

2.4.1 ACQUIRING THE ORACLE SHRINKAGE α

Estimating the oracle shrinkage parameter α is crucial for constructing the personalized posterior predictive means and variances of the biomarker trajectory. To estimate α , we use a held-out set of subjects with known trajectories, unseen by the population model. Predictions for these subjects are generated using the p-DKGP model. For each subject, the ss-DKGP component is trained by progressively increasing the length of the observed trajectory.

The entire biomarker trajectory is reconstructed from the baseline time ($t = 0$) to the subject's last time point t_n . Using both models, p-DKGP and ss-DKGP, we obtain two estimates of the biomarker trajectory along with their predictive variances. Let Y_p and V_p denote the p-DKGP predictive mean and variance, and Y_s and V_s denote the ss-DKGP model predictive mean and variance. Let Y represent the ground truth biomarker values over time. The oracle α is estimated by minimizing the following criterion:

$$J_{s|h}(\alpha) = \sum_{t=0}^{t_n} (y_t - (\alpha \cdot y_{p_t} + (1 - \alpha) \cdot y_{s_t}))^2. \quad (10)$$

The notation $J_{s|h}$ reflects that this optimization is performed for a subject s , given h observed acquisitions. The algorithm for calculating the oracle shrinkage estimates on the validation set is outlined in Algorithm 1. Each subject’s data is processed individually, applying the optimization to each sequence of observations. This process is repeated for every subject in the validation set.

Algorithm 1 Oracle Shrinkage Estimation

Require: Validation set $V = \{(U^s, Y^{(s)}) \mid s \in S\}$, where $Y^{(s)} = \{y_t^{(s)}\}_{t=1}^T$ is the ground truth trajectory for subject s

Ensure: Optimal shrinkage parameters $\hat{\alpha}_{s,h}$ for each $s \in S$ and $h \in H$

- 1: **for** each $s \in S$ **do**
- 2: Initialize list $L^{(s)} \leftarrow []$
- 3: **for** each $h \in H$ **do**
- 4: Obtain p-DKGP trajectory: $Y_p^{(s,h)} = \{y_{p,t}^{(s,h)}\}_{t=1}^T$
- 5: Obtain ss-DKGP trajectory: $Y_s^{(s,h)} = \{y_{s,t}^{(s,h)}\}_{t=1}^T$
- 6: Define objective function:

$$J_{s,h}(\alpha) = \sum_{t=0}^T \left(y_t^{(s)} - \left(\alpha y_{p,t}^{(s,h)} + (1 - \alpha) y_{s,t}^{(s,h)} \right) \right)^2$$

- 7: Compute:

$$\hat{\alpha}_{s,h} = \arg \min_{\alpha \in [0,1]} J_{s,h}(\alpha)$$

- 8: Append $\hat{\alpha}_{s,h}$ to $L^{(s)}$
 - 9: **end for**
 - 10: Store list $L^{(s)}$ for subject s
 - 11: **end for**
-

2.4.2 LEARNING THE ADAPTIVE SHRINKAGE α

The shrinkage parameter α represents the trust factor between the two components (p-DKGP and ss-DKGP). We model α as a function of the input variables $q = \{y_p, y_s, v_p, v_s, T_{\text{obs}}\}$, where $q \in \mathbb{R}^5$ and T_{obs} represents the time of observation. Using oracle shrinkage α obtained from Section 2.4.1) on the validation set, our objective is to learn a mapping function g_a that transforms the input space $q \in \mathbb{R}^5$, to the output space of adaptive shrinkage $\alpha \in \mathbb{R}$, as $\hat{\alpha} = g_a(q; \theta)$.

We employ XGBoost regression to learn the function g that minimizes the difference between the predicted $\hat{\alpha}$ and the oracle α . The learned function is denoted as g_α . In Supplementary Section C.2, we provide results from additional non-linear functions we experiment with, demonstrating that XGBoost achieves the best performance for estimating the shrinkage α .

2.5 PERSONALIZATION THROUGH ADAPTIVE SHRINKAGE ESTIMATION

For a new test subject with h observations and T_{obs} as the observation time (measured from the subject’s first visit), we train the ss-DKGP model as described in Section 2.3. The posterior-corrected predictive distribution, referred to as pers-DKGP, is computed using the following algorithm:

Algorithm 2 Personalization through Adaptive Shrinkage Estimation

Require: p-DKGP model, ss-DKGP model, and learned function g_α

Ensure: Adapted predictive mean and variance: Y_c, V_c

- 1: Compute Y_p, V_p (predictive mean and variance) from the p-DKGP model.
 - 2: Compute Y_s, V_s (predictive mean and variance) from the ss-DKGP model.
 - 3: Estimate shrinkage parameter: $\hat{\alpha}_h = g_\alpha(Y_p, Y_s, V_p, V_s, T_{\text{obs}})$.
 - 4: Compute the adapted predictive mean: $Y_c = \hat{\alpha}_h \cdot Y_p + (1 - \hat{\alpha}_h) \cdot Y_s$.
 - 5: Compute the adapted predictive variance: $V_c = \hat{\alpha}_h^2 \cdot V_p + (1 - \hat{\alpha}_h)^2 \cdot V_s$.
 - 6: **return** Y_c, V_c .
-

The personalization process through Adaptive Shrinkage Estimation is described in Algorithm 2.

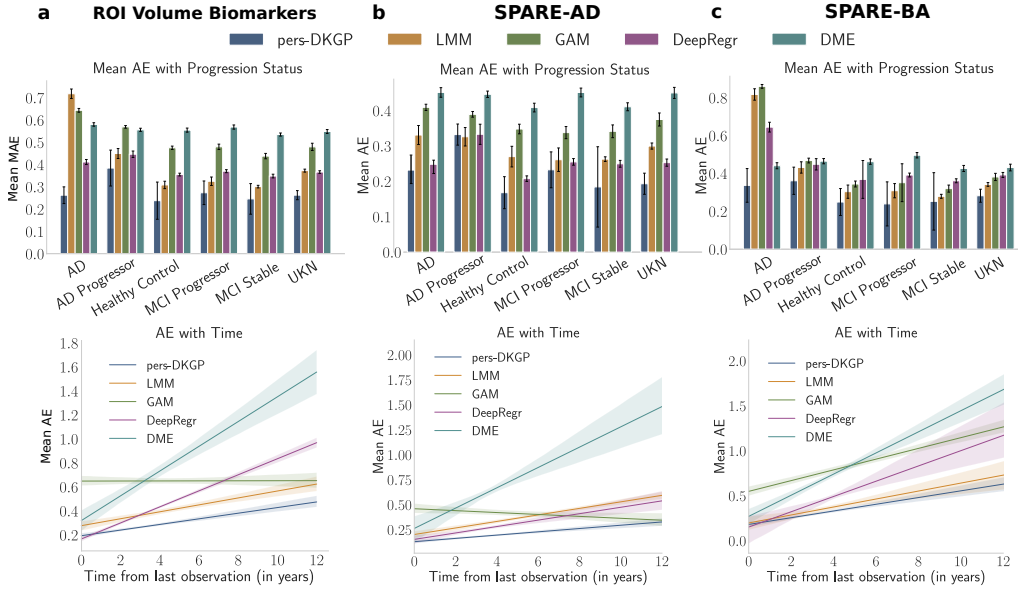


Figure 2: We compare the mean MAE per subject stratified by the progression status (top) and the AE with time from the last observation (bottom) of our method with the baselines for (a) the 7 ROI Volume biomarkers, (b) SPARE-AD score and (c) SPARE-BA. Error bars, in the top row, denote the 95th percentile of the MAE across all subjects. Our method is denoted as pers-DKGP.

3 EXPERIMENTS

3.1 PREDICTION OF REGIONAL VOLUMETRIC TRAJECTORIES

In this section, we apply deep kernel regression with Adaptive Shrinkage Estimation to predict trajectories of seven volumetric Regions of Interest (ROI): Hippocampus R, Hippocampus L, Thalamus Proper R, Amygdala R, Amygdala L, Parahippocampal Gyrus R and Lateral Ventricle R. For each ROI Volume model we use a dataset of 2,200 subjects with $U_i = (X_i, M_i, T_i)$ from subject i , where X_i are volumetric measures from 145 brain regions collected at subjects’s first visit, M_i are the covariates of diagnosis at subject’s first visit, sex, age, education, APOE4 Alleles, a genetic variant related to AD and T_i is the time from subject’s first visit. For each ROI Volume biomarker, the p-DKGP model is trained on a population cohort of 1,600 subjects, while the adaptive shrinkage estimator is trained on a held-out set of 200 subjects. Predictive performance is evaluated on 440 test subjects. For details on the architecture and training of the ROI Volume deep kernel models, p-DKGP and ss-DKGP, see Section B.1.

We combine preprocessed and harmonized neuroimaging measures from two well-known longitudinal studies: the Alzheimer’s Disease Neuroimaging Initiative (ADNI) (Weiner et al., 2017) and the Baltimore Longitudinal Study of Aging (BLSA) (Ferrucci, 2008), which focus on Alzheimer’s Disease and Brain Aging, respectively. Further details on the studies and preprocessing pipelines are provided in Supplementary Section A.

We benchmark our method against several baselines and state-of-the-art predictors: Linear Mixed Model (LMM) (Lindstrom & Bates, 1988), Generalized Additive Model (GAM) (Hastie & Tibshirani, 1986), Deep Neural Network Regression, and the Deep Mixed Effects (DME) (Chung et al., 2019). Further details on the architectural design and training of baselines are provided in Supplementary B.3. Model performance is evaluated from two perspectives: predictive accuracy and uncertainty quantification (UQ). Predictive accuracy is measured using Absolute Error (AE) and Mean Absolute Error (MAE) per subject. UQ is assessed by interval width (the range between ± 2 standard deviations from the predictive mean) and coverage (the proportion of true biomarker values within that range). Importantly, these metrics are computed over the entire unseen trajectory of test subjects, providing a comprehensive evaluation of model performance over time. We refer to our method as personalized-DKGP or shortly pers-DKGP.

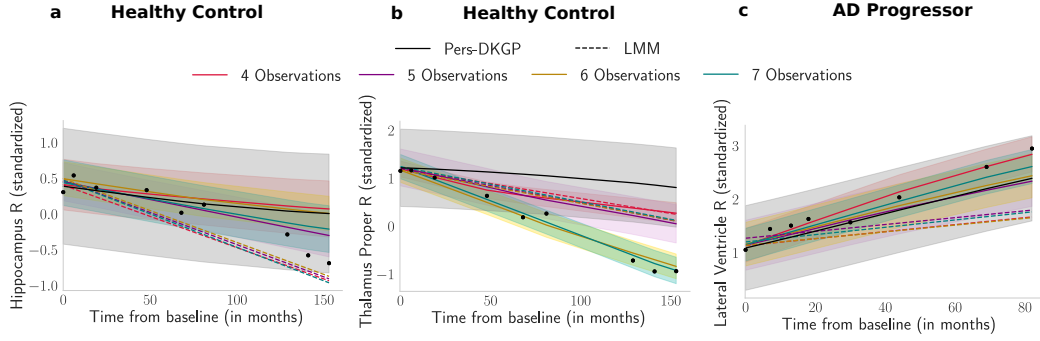


Figure 3: We present personalized ROI volume trajectories for three test subjects as observations increase from 4 to 7 acquisitions. The dashed lines represent the prediction using LMM. The first two panels visualize the Hippocampus R and Thalamus Proper R Volume trajectories of Healthy Control subject. Last panel shows the Lateral Ventricle R Volume for an AD Progressor. The shaded bands represent the predictive uncertainty over time.

For each predictor, Figure 2a presents a comparative study of the predictive performance with respect to progression status and time from the last known acquisition. Progression status is defined by the subject’s initial and final diagnoses, categorized as follows: AD refers to subjects diagnosed with AD at their first visit; AD Progressor includes subjects initially diagnosed as Cognitively Normal (CN) or Mild Cognitively Impaired (MCI) who progress to AD; Healthy Controls are subjects who remain CN throughout all visits; MCI Progressor refers to subjects who progress from CN to MCI; MCI Stable includes subjects who remain MCI throughout their trajectory; and Unknown (UKN) corresponds to cases involving misdiagnosis.

Building on this categorization, Figure 2a shows the mean MAE across progression status for the seven volumetric ROIs. Notably, the largest mean MAE differences between our method and baselines occur in participants with AD and AD Progressors, who exhibit non-linear and steeper trends that competing baselines fail to capture. Specifically, the Linear Mixed Model (LMM), constrained to linear patterns in ROI volumes, shows significant percentage mean MAE differences in AD (177.66%) and AD progressors (22.05%). Even in healthy controls, LMM exhibits a 29.78% MAE difference, highlighting its inability to capture trajectories even in cases of relatively stable volume trajectories. Further quantitative comparisons, including error stratification by covariates such as sex, APOE4 Alleles, and education years, are provided in Supplementary Sections D.1.

In addition to evaluating performance with respect to progression status, we also assess the model’s ability to predict long-term longitudinal trajectories. In Figure 2a, we visualize the mean AE across different lengths of observed trajectories, with errors plotted relative to the time from the last observation. Our method achieves progressively lower mean AE over time, indicating improved precision in both long-term and short-term predictions. This demonstrates the model’s ability in capturing temporal trends and adapting to varying observation lengths.

To further highlight the strengths of our model, we provide a qualitative evaluation of the predicted trajectories in Figure 3. For the Volume ROIs of Hippocampus R, Thalamus Proper R, and Lateral Ventricle R, our model successfully adapts to the observed trajectories of test subjects, resulting in more accurate long-term predictions. For instance, in the Healthy Control subject shown in Figure 3b, the population prediction deviates from the actual trajectory. However, as the number of observations increases, the pers-DKGP trajectory shifts toward the observed trajectory, effectively adapting to the subject-specific trend. Similarly, the third subject, an AD Progressor in Figure 3c, exhibits an abrupt increase in ventricular volume. This trend is captured with few observations by the pers-DKGP model, while the LMM underestimates the ventricular volume in the long term. Additional qualitative examples of trajectories are provided in Supplementary Section D.3.

Overall, the LMM exhibits limited flexibility in capturing non-linear patterns in ROI volumes, rendering it inadequate for long-term biomarker prediction. While it performs reasonably well in short-term forecasts and lower-dimensional settings, its expressiveness falls short for complex, high-dimensional inputs. Deep regression, though capable of learning from observed data, often

yields non-smooth or non-monotonic trajectories that deviate from biologically plausible biomarker progression trends. The DME model, which combines a shared deep mean function with subject-specific GP, struggles to achieve personalization in high-dimensional input spaces, resulting in persistent errors across time and diagnostic categories. These issues stem from the limitations of the RBF kernel in managing multivariate, high-dimensional data. In contrast, our method effectively approximates non-linear mixed effects models, demonstrating flexibility in handling multivariate, high-dimensional data and capturing diverse temporal patterns.

3.2 APPLICATION TO NEUROIMAGING BIOMARKERS: SPARE SCORES

Having demonstrated our framework’s ability to personalize longitudinal predictions of volumetric ROIs as subject observations increase, we now show its versatility by applying it to composite neuroimaging biomarkers: the SPARE-AD (Davatzikos et al., 2009) and SPARE-BA (Habes et al., 2016) scores. SPARE-AD quantifies the risk of AD progression, while SPARE-BA represents predicted brain age. For both SPARE models we use a dataset of 2,200 subjects with $U_i = (X_i, M_i, T_i)$ from subject i , where X_i are volumetric measures from 145 brain regions collected at subjects’s first visit, M_i are the covariates of diagnosis at subject’s first visit, sex, age, education, APOE4 Alleles, the SPARE-AD and SPARE-BA values at the first visit and T_i is the time from subject’s first visit. The p-DKGP model is trained on 1600 subjects, the adaptive shrinkage estimator is trained on a held-out set of 200 subjects. The evaluation of the predictive performance is performed on the 440 test subjects. For details on the architectural design and training of the SPARE-AD and SPARE-BA deep kernel models (p-DKGP and ss-DKGP) see Section B.2.

Our model demonstrates strong performance in predicting long-term longitudinal trajectories for both SPARE-AD and SPARE-BA biomarkers, as illustrated in Figure 2b and 2c. Notably, the model achieves progressively lower mean AE over time, indicating improved precision in forecasting long-term outcomes. For SPARE-BA, model performance differences are minimal in stable subjects and healthy controls, but more pronounced in AD subjects, where SPARE-BA exhibits steeper progression trends due to accelerated brain aging. For the SPARE-AD biomarker, we also visualize absolute error with the number of observations. This highlights how our model adapts with increasing observations, starting with a single scan using the p-DKGP model ($\alpha = 1$) and transitioning to adapted shrinkage estimation for personalization as follow-up observations increase. Evidence is provided in Table 5 and Figure 7 in Supplementary Section D.2.

3.3 APPLICATION TO EXTERNAL NEUROIMAGING STUDIES

In this section, we demonstrate the generalizability of our method to previously unseen neuroimaging datasets. After training the p-DKGP and adaptive shrinkage estimator on the population and validation datasets from the ADNI and BLSA cohorts, we personalize starting from the first follow-up point for each subject and predict the remaining trajectory. This process is repeated for all follow-up points, with the very last follow-up reserved for testing.

We test the performance of our framework on subjects from three independent clinical studies: OASIS (Marcus et al., 2010), AIBL (Ellis et al., 2009), and PreventAD (Tremblay-Mercier et al., 2021). These datasets differ from the training population in terms of demographics, diagnosis composition, and follow-up intervals, presenting a challenging test of the model’s generalizability across diverse populations. In Supplementary Section A we present details on the demographic and clinical characteristics of these studies.

The three external studies exhibit notable differences in demographics and follow-up intervals: **AIBL**: Includes 82 individuals with a mean age of 75 years, which is close to the mean age of the joint cohort of ADNI and BLSA. It is predominantly composed of AD patients followed by MCI and Healthy Controls. On average, each subject has approximately 3 follow-up visits, with a mean interval of 24 months between visits. **OASIS**: Includes 559 individuals younger on average (67.8 years) compared to both ADNI and BLSA. It is primarily composed of healthy controls, with smaller representations of MCI and AD cases. The average number of follow-ups is ~ 3 per subject, with a mean interval of 32 months. **PreventAD**: Includes 271 individuals and focuses on pre-symptomatic early detection of AD in a healthier and younger population (mean age 65.3 years) with an average of 4 follow-up visits per subject and a shorter mean interval of 10 months.

Our method outperforms baseline predictors across three independent clinical studies—AIBL, OASIS, and PreventAD—underscoring its effectiveness in diverse, real-world scenarios (Figure 4). The model achieves lower MAE compared to baselines, with narrow confidence intervals reflecting its

stability. In the AIBL study, pers-DKGP achieves a Mean AE of 0.197 ± 0.009 , substantially outperforming the baseline methods. A similar trend is observed in the OASIS study, where pers-DKGP attains a Mean AE of 0.259 ± 0.006 . Notably, in the PreventAD study, our method achieves the lowest Mean AE of 0.139 ± 0.004 , outperforming LMM and GAM. The narrow CIs of the AE associated with pers-DKGP across all datasets highlight its reliability and consistent precision, even in the presence of data variability. Interestingly, the lowest error observed in the PreventAD study, along with the reduced disparity between pers-DKGP and statistical models like LMM and GAM, is attributed to the younger population and shorter follow-up intervals in this dataset. Predicting Volume ROIs in a younger, healthier control population, as in PreventAD, is inherently less challenging compared to the older, partially demented populations in OASIS and AIBL.

Collectively, these results position our model as a robust and reliable framework for personalized forecasting of neuroimaging biomarkers, offering potential for application in clinical trials and neuroimaging studies.

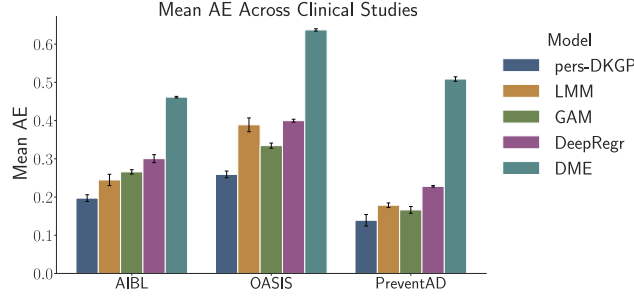


Figure 4: We evaluate the mean absolute error for the seven ROI Volume biomarkers across three external neuroimaging studies. Error bars denote the 95th percentile of the absolute error. Notice that the pers-DKGP achieves the lower error across all external studies, in comparison with the competing baselines.

3.4 EXPLAINING ADAPTIVE SHRINKAGE: AN ABLATION STUDY ON THE α FUNCTION

In this section, we demonstrate the effectiveness and interpretability of the Adaptive Shrinkage estimator. We first compare it to alternative posterior correction approaches and then use explainability analysis to illustrate how Adaptive Shrinkage learns to balance the two posterior predictive distributions in a data-driven manner, making its decision-making process intuitive.

We explore various strategies for selecting the shrinkage parameter α . First, we experiment with a constant $\alpha = c$, where $c \in (0, 1)$, representing an uninformative approach to posterior correction. Next, we employ a semi-informative (deterministic) approach, where the α for each test subject is determined by optimizing the objective in Equation 10 using only subject’s observed trajectory. Finally, we use adaptive shrinkage estimator to determine α . We conduct this experiment for seven ROI Volume biomarkers: Hippocampus R/L, Lateral Ventricle, Thalamus Proper, Amygdala R/L, and the Parahippocampal Gyrus (PHG R). The deterministic method results in the worst outcomes in terms of both predictive performance and uncertainty quantification, suggesting that the observed trajectory alone is insufficient to determine the α for future predictions. Here, we present results for Hippocampus R, Lateral Ventricle, and Thalamus Proper under the constant α and Adaptive Shrinkage. Results for the remaining Volume ROIs are provided in Table 6 of Supplementary Section D.4.1.

In the constant α section of Table 1, we present the performance of the best constant α values. This demonstrates that optimal performance is not achieved through simple averaging and that the optimal α varies significantly across ROIs. For example, the best α is 0.5 for Hippocampus, 0.3 for Lateral Ventricle, and 0.7 for Thalamus Proper. These results highlight the inadequacy of a one-size-fits-all approach and underscore the necessity for a more sophisticated method. The evidence suggests that Adaptive Shrinkage provides a more informed approach for determining the ideal α , leading to improved predictive performance and uncertainty quantification.

To elucidate the decision-making process of Adaptive Shrinkage, we conduct explainability analysis. We focus on the impact of each input variable— Y_p , Y_s , V_p , V_s , and T_{obs} —and their interactions on the prediction of the adaptive shrinkage parameter α . Specifically, we aim to understand how the

Table 1: Ablation study on the shrinkage parameter α . We report the Mean AE along with its 95% percentile CI, Mean Coverage, and Mean Interval Width

ROI	α	Best Constant			Adaptive Shrinkage		
		Mean AE (CI)	Mean Cov.	Mean Int.	Mean AE (CI)	Mean Cov.	Mean Int.
Hippocampus R	0.5	0.257 (± 0.007)	0.808	0.843	0.243 (± 0.003)	0.795	0.902
Lateral Ventricle R	0.3	0.143 (± 0.006)	0.853	0.507	0.131 (± 0.002)	0.855	0.626
Thalamus Proper R	0.7	0.241 (± 0.007)	0.934	1.127	0.219 (± 0.003)	0.849	0.911

deviation between the population and subject-specific predictive means ($\delta_y = Y_p - Y_s$) and the observation time T_{obs} influence the model’s predictions.

We employ SHAP (SHapley Additive exPlanations) values (Lundberg & Lee, 2017) to interpret the contribution of each feature to individual predictions. Figure 13 in Supplementary Section D.4 reveals that T_{obs} is the most influential variable in the decision-making process. This is further validated by the observation that the distribution of adaptive shrinkage α decreases as the number of follow-up observations (and thus T_{obs}) increases. Figure 12 in Supplementary Section D.4 demonstrates the distribution of α with the number of observations for the seven ROIs and SPARE scores, as well as the adaptive shrinkage α obtained from external neuroimaging studies. The consistent trend of decreasing α as the number of observations increases highlights the biomarker-agnostic ability of Adaptive Shrinkage to optimally combine population and subject-specific trends. This behavior is also consistent across external neuroimaging studies, further validating the generalizability of the approach. Additional qualitative results demonstrating the decision-making process of Adaptive Shrinkage are provided in Supplementary Section D.3, Figures 10 and 11.

Furthermore, correlation analysis (Supplementary Section D.4, Table 7) reveals a consistent negative relationship between T_{obs} and the predicted α when the deviation δ_y is large. This indicates that, in the presence of significant deviations between the two predictors, Adaptive Shrinkage reduces the weight assigned to the population-level model (p-DKGP) for longer observation periods. This aligns with the intuition that as more follow-up observations are available, greater trust is placed in the subject-specific predictive distribution.

4 DISCUSSION

In this paper, we introduce deep kernel regression with adaptive shrinkage estimation for predicting personalized biomarker trajectories via posterior correction. Our method learns the adaptive shrinkage parameter that effectively combines two posterior predictive distributions, enabling the predictive trajectory to adapt to each subject’s follow-up acquisitions. Additionally, our method is versatile, effectively modeling the progression of longitudinal biomarkers using multivariate imaging data and clinical covariates. Examples of such biomarkers are the cognitive scores (e.g., MMSE, ADAS-Cog13) and blood biomarkers (e.g., Amyloid- β , Tau protein). Importantly, our approach exhibits generalization capabilities when applied to external neuroimaging studies with diverse demographics and follow-up intervals, which is particularly valuable for real-world applications, where models must perform robustly across heterogeneous populations.

Such property is particularly important as the use of predictive models in healthcare is increasingly critical for both patient management and drug development. Cummings et al. (2019) emphasize the need for AI-informed clinical trials, referred to as precision trial design, while Maheux et al. (2023) evaluate predictive models for biomarker trajectories in Alzheimer’s Disease, where derived measures—such as the rate of change—serve as quantitative indicators of disease progression during clinical trials. These measures inform decisions on subject inclusion and treatment efficacy, underscoring the importance of reliable and interpretable predictive tools. Our method’s adaptive and intuitive design positions it as a valuable tool for clinical trial design, disease progression modeling, treatment effect estimation, and neuroimaging research. By leveraging personalized predicted brain ROIs and neuroimaging biomarkers, such as SPARE-AD, as endpoints for selecting trial subjects, our framework showcases its potential for real-world application.

At the same time, we acknowledge limitations in our approach, particularly the independence assumption between the α parameter and posterior distributions in the posterior correction step (Supplementary Section 2.4). While this simplification impacts uncertainty quantification, it does not

affect the posterior-corrected predictive mean, ensuring accurate predictions. Further discussion on this assumption, including its theoretical justification and potential implications, is provided in Supplementary Section C. Future work will explore extending adaptive shrinkage to multivariate biomarker trajectories and improving uncertainty quantification in personalized trajectories to address this aforementioned limitation.

REFERENCES

- Clément Abi Nader, Nicholas Ayache, Philippe Robert, and Marco Lorenzi. Monotonic Gaussian Process for spatio-temporal disease progression modeling in brain imaging data. *NeuroImage*, 205:116266, 2020. ISSN 1053-8119. doi: <https://doi.org/10.1016/j.neuroimage.2019.116266>. URL <https://www.sciencedirect.com/science/article/pii/S1053811919308572>.
- Jorge L. Bernal-Rusiel, Douglas N. Greve, Martin Reuter, Bruce Fischl, Mert R. Sabuncu, and Alzheimer’s Disease Neuroimaging Initiative. Statistical analysis of longitudinal neuroimage data with Linear Mixed Effects models. *NeuroImage*, 66:249–260, 2013. doi: 10.1016/j.neuroimage.2012.10.065. Epub 2012 Oct 30. Erratum in: *Neuroimage*. 2015 Mar;108:110. PMID: 23123680; PMCID: PMC3586747.
- Ingyo Chung, Saehoon Kim, Juho Lee, Kwang Joon Kim, Sung Ju Hwang, and Eunho Yang. Deep Mixed Effect Model using Gaussian Processes: A Personalized and Reliable Prediction for Healthcare, 2019. URL <https://arxiv.org/abs/1806.01551>.
- Jeffrey Cummings, Howard H. Feldman, and Philip Scheltens. The “rights” of precision drug development for Alzheimer’s disease. *Alzheimer’s Research & Therapy*, 11:76, 2019. doi: 10.1186/s13195-019-0529-5.
- Christos Davatzikos, Feng Xu, Yang An, Yong Fan, and Susan M. Resnick. Longitudinal progression of alzheimer’s-like patterns of atrophy in normal older adults: the spare-ad index. *Brain*, 132(8): 2026–2035, August 2009. doi: 10.1093/brain/awp091. URL <https://doi.org/10.1093/brain/awp091>.
- Jimit Doshi, Guray Erus, Yangming Ou, Susan M. Resnick, Ruben C. Gur, Raquel E. Gur, Theodore D. Satterthwaite, Susan Furth, and Christos Davatzikos. MUSE: MULti-atlas region Segmentation utilizing Ensembles of registration algorithms and parameters, and locally optimal atlas selection. *NeuroImage*, 127:186–195, 2 2016. ISSN 10959572. doi: 10.1016/j.neuroimage.2015.11.073.
- Kathryn A. Ellis, Ashley I. Bush, David Darby, Daniela De Fazio, Jonathan Foster, Peter Hudson, Nicola T. Lautenschlager, Nat Lenzo, Ralph N. Martins, Paul Maruff, Colin Masters, Andrew Milner, Kerry Pike, Christopher Rowe, Greg Savage, Cassandra Szeke, Kevin Taddei, Victor Villemagne, Michael Woodward, and David Ames. The Australian Imaging, Biomarkers and Lifestyle (aibl) study of aging: methodology and baseline characteristics of 1112 individuals recruited for a longitudinal study of Alzheimer’s disease. *International Psychogeriatrics*, 21(4): 672–687, 2009. doi: 10.1017/S1041610209009405. URL <https://pubmed.ncbi.nlm.nih.gov/19470201/>.
- Luigi Ferrucci. The Baltimore Longitudinal Study of Aging (BLSA): A 50-year-long journey and plans for the future. *The Journals of Gerontology: Series A: Biological Sciences and Medical Sciences*, 63(12):1416–1419, 2008. doi: 10.1093/gerona/63.12.1416.
- Samuel Gruffaz, Pierre-Emmanuel Poulet, Etienne Maheux, Bruno Jedynak, and Stanley DURLÉMAN. Learning Riemannian metric for disease progression modeling. In M. Ranzato, A. Beygelzimer, Y. Dauphin, P.S. Liang, and J. Wortman Vaughan (eds.), *Advances in Neural Information Processing Systems*, volume 34, pp. 23780–23792. Curran Associates, Inc., 2021. URL https://proceedings.neurips.cc/paper_files/paper/2021/file/c7b90b0fc23725f299b47c5224e6ec0d-Paper.pdf.
- Mohamad Habes, Deborah Janowitz, Guray Erus, Jon B. Toledo Atucha, Susan M. Resnick, Jimit Doshi, Sandra van der Auwera, Katharina Wittfeld, Katrin Hegenscheid, Norbert Hosten, Reiner

- Biffar, Georg Homuth, Henry Völzke, Hans J. Grabe, Wolfgang Hoffmann, and Christos Davatzikos. Advanced brain aging: relationship with epidemiologic and genetic risk factors, and overlap with Alzheimer disease atrophy patterns. *Translational Psychiatry*, 6(4):e775, 2016. doi: 10.1038/tp.2016.39. PMID: 27045845; PMCID: PMC4872397.
- Mohamad Habes, Raymond Pomponio, Haochang Shou, Jimit Doshi, Elizabeth Mamourian, Guray Erus, Ilya Nasrallah, Lenore J Launer, Tanweer Rashid, Murat Bilgel, et al. The Brain Chart of Aging: machine-learning analytics reveals links between brain aging, white matter disease, amyloid burden, and cognition in the iSTAGING consortium of 10,216 harmonized MR scans. *Alzheimer's & Dementia*, 17(1):89–102, 2021.
- Trevor Hastie and Robert Tibshirani. Generalized Additive Models. *Statistical Science*, 1(3):297–310, 1986. URL <http://www.jstor.org/stable/2245459>.
- Sepp Hochreiter and Jürgen Schmidhuber. Long short-term memory. *Neural Computation*, 9(8): 1735–1780, 1997.
- Sungmin Hong, James Fishbaugh, Jason J. Wolff, Martin A. Styner, and Guido Gerig. Hierarchical multi-geodesic model for longitudinal analysis of temporal trajectories of anatomical shape and covariates. In *Medical Image Computing and Computer-Assisted Intervention – MICCAI 2019*, volume 11767, pp. 57–65. Springer, Oct 2019. doi: 10.1007/978-3-030-32251-9_7. URL https://doi.org/10.1007/978-3-030-32251-9_7.
- Willard James and Charles Stein. Estimation with quadratic loss. In *Proceedings of the Third Berkeley Symposium on Mathematics. Statistics and Probability*, volume 1, 1961.
- Diederik P. Kingma and Jimmy Ba. Adam: A Method for Stochastic Optimization. *CoRR*, abs/1412.6980, 2014. URL <https://api.semanticscholar.org/CorpusID:6628106>.
- Igor Koval, Alexandre Bône, Maxime Louis, Thomas Lartigue, Simona Bottani, Arnaud Marcoux, Jorge Samper-González, Ninon Burgos, Benjamin Charlier, Anne Bertrand, et al. AD Course Map charts Alzheimer’s disease progression. *Scientific Reports*, 2021. Available at Inria - Institut national de recherche en sciences et technologies du numérique (HAL).
- Mary J. Lindstrom and Douglas M. Bates. Newton-Raphson and EM Algorithms for Linear Mixed-Effects Models for Repeated-Measures Data. *Journal of the American Statistical Association*, 83(404):1014–1022, 1988. doi: 10.2307/2290124. URL <https://www.jstor.org/stable/2290124>.
- Marco Lorenzi, Maurizio Filippone, Giovanni B. Frisoni, Daniel C. Alexander, and Sebastien Ourselin. Probabilistic disease progression modeling to characterize diagnostic uncertainty: Application to staging and prediction in Alzheimer’s disease. *NeuroImage*, 190:56–68, April 2019. ISSN 1053-8119. doi: 10.1016/j.neuroimage.2017.08.059. URL <http://dx.doi.org/10.1016/j.neuroimage.2017.08.059>.
- Scott M Lundberg and Su-In Lee. A Unified Approach to Interpreting Model Predictions. In I. Guyon, U. Von Luxburg, S. Bengio, H. Wallach, R. Fergus, S. Vishwanathan, and R. Garnett (eds.), *Advances in Neural Information Processing Systems*, volume 30. Curran Associates, Inc., 2017. URL https://proceedings.neurips.cc/paper_files/paper/2017/file/8a20a8621978632d76c43dfd28b67767-Paper.pdf.
- Etienne Maheux, Igor Koval, Juliette Ortholand, Colin Birkenbihl, Damiano Archetti, Vincent Bouteloup, Stéphane Epelbaum, Carole Dufouil, Martin Hofmann-Apitius, and Stanley Durrleman. Forecasting individual progression trajectories in Alzheimer’s disease. *Nature Communications*, 14(1):1–15, 2023. doi: 10.1038/s41467-022-35712-5.
- Daniel S. Marcus, Anthony F. Fotenos, John G. Csernansky, John C. Morris, and Randy L. Buckner. Open Access Series of Imaging Studies: Longitudinal MRI Data in Nondemented and Demented Older Adults. *Journal of Cognitive Neuroscience*, 22(12):2677–2684, 12 2010. ISSN 0898-929X. doi: 10.1162/jocn.2009.21407. URL <https://doi.org/10.1162/jocn.2009.21407>.

- Razvan V. Marinescu, Neil P. Oxtoby, Alexandra L. Young, Esther E. Bron, Arthur W. Toga, Michael W. Weiner, Frederik Barkhof, Nick C. Fox, Stefan Klein, Daniel C. Alexander, and the EuroPOND Consortium. Tadpole challenge: Prediction of longitudinal evolution in alzheimer’s disease, 2018. URL <https://arxiv.org/abs/1805.03909>.
- Richard C. Mohs, David Knopman, Ronald C. Petersen, Steven H. Ferris, Claudia Ernesto, Michael Grundman, Mary Sano, Lee Bieliauskas, David Geldmacher, Christopher Clark, and Leon J. Thal. Development of cognitive instruments for use in clinical trials of antidementia drugs: additions to the Alzheimer’s Disease Assessment Scale that broaden its scope. the Alzheimer’s Disease Cooperative Study. *Alzheimer Disease and Associated Disorders*, 11 Suppl 2:S13–S21, 1997.
- Raymond Pomponio, Guray Erus, Mohamad Habes, Jimit Doshi, Dhivya Srinivasan, Elizabeth Mamourian, Vishnu Bashyam, Ilya M Nasrallah, Theodore D Satterthwaite, Yong Fan, et al. Harmonization of large mri datasets for the analysis of brain imaging patterns throughout the lifespan. *NeuroImage*, 208:116450, 2020.
- Carl Edward Rasmussen and Christopher K. I. Williams. *Gaussian Processes for Machine Learning*. MIT Press, 2006.
- Ognjen (Oggi) Rudovic, Yuria Utsumi, Ricardo Guerrero, Kelly Peterson, Daniel Rueckert, and Rosalind W. Picard. Meta-Weighted Gaussian Process Experts for Personalized Forecasting of AD Cognitive Changes. In Finale Doshi-Velez, Jim Fackler, Ken Jung, David Kale, Rajesh Ranganath, Byron Wallace, and Jenna Wiens (eds.), *Proceedings of the 4th Machine Learning for Healthcare Conference*, volume 106 of *Proceedings of Machine Learning Research*, pp. 181–196. PMLR, 09–10 Aug 2019. URL <https://proceedings.mlr.press/v106/rudovic19a.html>.
- Mert R. Sabuncu, Juan L. Bernal-Rusiel, Martin Reuter, Douglas N. Greve, and Bruce Fischl. Event time analysis of longitudinal neuroimage data. *Neuroimage*, 97:9–18, 2014. doi: 10.1016/j.neuroimage.2014.04.015.
- Haochang Shou, Ani Eloyan, Mary Beth Nebel, Amanda Mejia, James J. Pekar, Stewart Mostofsky, Brian Caffo, Martin A. Lindquist, and Ciprian M. Crainiceanu. Shrinkage prediction of seed-voxel brain connectivity using resting state fMRI. *NeuroImage*, 102(Pt 2):938–944, 2014.
- Vasiliki Tassopoulou, Fanyang Yu, and Christos Davatzikos. Deep Kernel Learning with Temporal Gaussian Processes for Clinical Variable Prediction in Alzheimer’s Disease. In Antonio Parziale, Monica Agrawal, Shalmali Joshi, Irene Y. Chen, Shengpu Tang, Luis Oala, and Adarsh Subbaswamy (eds.), *Proceedings of the 2nd Machine Learning for Health symposium*, volume 193 of *Proceedings of Machine Learning Research*, pp. 539–551. PMLR, 28 Nov 2022. URL <https://proceedings.mlr.press/v193/tassopoulou22a.html>.
- Jennifer Tremblay-Mercier, Cécile Madjar, Samir Das, Alexa Pichet Binette, Stephanie O. M. Dyke, Pierre Étienne, Marie-Elyse Lafaille-Magnan, Jordana Remz, Pierre Bellec, D. Louis Collins, M. Natasha Rajah, Veronique Bohbot, Jeannie-Marie Leoutsakos, Yasser Iturria-Medina, Justin Kat, Richard D. Hoge, Serge Gauthier, Christine L. Tardif, M. Mallar Chakravarty, Jean-Baptiste Poline, Pedro Rosa-Neto, Alan C. Evans, Sylvia Villeneuve, Judes Poirier, John C. S. Breitner, and PREVENT-AD Research Group. Open science datasets from PREVENT-AD, a longitudinal cohort of pre-symptomatic Alzheimer’s disease. *NeuroImage: Clinical*, 31:102733, 2021. doi: 10.1016/j.nicl.2021.102733.
- Ashish Vaswani, Noam Shazeer, Niki Parmar, Jakob Uszkoreit, Llion Jones, Aidan N. Gomez, Łukasz Kaiser, and Illia Polosukhin. Attention Is All You Need. In *Advances in Neural Information Processing Systems*, volume 30, pp. 5998–6008, 2017.
- Michael W. Weiner, Dallas P. Veitch, Paul S. Aisen, Laurel A. Beckett, Nigel J. Cairns, Robert C. Green, Danielle Harvey, Clifford R. Jack, William Jagust, John C. Morris, Ronald C. Petersen, Andrew J. Saykin, Leslie M. Shaw, Arthur W. Toga, and John Q. Trojanowski. Recent publications from the Alzheimer’s Disease Neuroimaging Initiative: Reviewing progress toward improved AD clinical trials. *Alzheimer’s and Dementia*, 13:e1–e85, 4 2017. ISSN 15525279. doi: 10.1016/j.jalz.2016.11.007. URL <https://doi.org/10.1016/j.jalz.2016.11.007>.

Andrew Gordon Wilson, Zhiting Hu, Ruslan Salakhutdinov, and Eric P. Xing. Deep kernel learning, 2015. URL <https://arxiv.org/abs/1511.02222>.

Long Xie, Sandhitsu R. Das, Laura E. M. Wisse, Ranjit Ittyerah, Robin de Flores, Leslie M. Shaw, Paul A. Yushkevich, David A. Wolk, and for the Alzheimer’s Disease Neuroimaging Initiative. Baseline structural MRI and plasma biomarkers predict longitudinal structural atrophy and cognitive decline in early Alzheimer’s disease. *Alzheimer’s Research & Therapy*, 15(1):79, 2023. doi: 10.1186/s13195-023-01210-z. URL <https://doi.org/10.1186/s13195-023-01210-z>. Published: 2023/04/11.